Eur. Phys. J. B **70**, 497–505 (2009)
DOI: 10.1140/epjb/e2009-00247-7

THE EUROPEAN PHYSICAL JOURNAL B

Regular Article

Electron transport in nanotube-ribbon hybrids

T.S. Li[1,a], S.C. Chang[1], and M.F. Lin[2]

[1] Department of Electrical Engineering, Kun Shan University, Tainan, Taiwan, Republic of China
[2] Department of Physics, National Cheng Kung University, Tainan, Taiwan, Republic of China

Received 3 February 2009 / Received in final form 18 June 2009
Published online 18 August 2009 –

Abstract. The electronic and transport properties of nanotube-ribbon hybrids subject to the influences of a transverse electric field are investigated theoretically. The energy dispersion relations are found to exhibit rich dependence on the nanotube-ribbon interactions, the field strength, and the geometry of the hybrids. The nanotube-ribbon coupling will modify the subband curvature, create additional band-edge states, and change the subband spacing or energy gap. The bandstructures are asymmetric and symmetric about the Fermi energy when the interactions are turned on and off, respectively. The inclusion of a transverse electric field will further alter the bandstructures and lift the degeneracy of the partial flat bands in hybrid (IV). The chemical-potential-dependent electrical and thermal conductance exhibit a stepwise increase behavior. Variations in the electronic structures with field strength will be reflected in the electrical and thermal conductance. Prominent peaks, as well as single-shoulder and multi-shoulder structures in the electrical and thermal conductance are predicted when varying the electric field strength and the nanotube location. The features of the conductance are found to be strongly dependent on the field strength, the geometry and the temperature.

PACS. 73.23.-b Electronic transport in mesoscopic systems – 73.22.-f Electronic structure of nanoscale materials: clusters, nanoparticles, nanotubes, and nanocrystals

1 Introduction

Graphene, a flat monolayer of carbon atoms arranged in a two-dimensional honeycomb lattice, is the fundamental building block for graphitic materials of all other dimensionalities. Three-dimensional (3D) graphite is a stack of graphene layers. One-dimensional (1D) carbon nanotubes (CN's) [1–4] can be viewed as rolled-up cylinders of graphene. Zero-dimensional (0D) fullerenes [5] consist of wrapped graphene with introduction of pentagons into the hexagonal lattice. Recently, Novoselov and collaborators [6] succeeded in isolating single sheets of graphite known as graphene. Despite being only one atom thick, their graphene devices are stable under ambient conditions. Subsequent experiments [7–13] have demonstrated that it is feasible to modulate electrical properties of graphene devices by applying an external voltage, which opens up the possibility of graphene microelectronics. There are observations of unconventional electric field effects in the Hall coefficient [6], and novel quantum Hall effect in monolayer [12] and bilayer graphene [13]. These unusual electronic properties are due to the linear dispersion relation near the Dirac point. The carriers in graphene are massless Dirac fermions leading to the shifted Hall plateaus [8,12]. When graphene is patterned into a narrow ribbon, graphene nanoribbon (GNR) will then be obtained. Just like carbon nanotubes, graphene nanoribbons are also 1D systems. Graphene nanoribbons can be realized either by cutting mechanically exfoliated graphenes [12], or by patterning graphenes with lithographic techniques [7,14].

With the advance in chemical synthesis and scanning probe techniques, it has become possible to fabricate novel hybrid carbon materials. Fullerene peapods, formed by encapsulating C_{60} molecules in carbon nanotubes, were first observed by Smith and coworkers from transmission electron microscopy experiments [15]. This opens up the possibility to tailor different structures with the desired functionality. NanoBuds, consisting of fullerenes covalently attached to single-walled carbon nanotubes, have been synthesized by Nasibulin and coworkers [16]. Carbon nanowire, a multiwalled carbon nanotube which contains a single chain of carbon atoms encapsulated within the inner most tube, was reported [17]. Gutierrez and coworkers proposed an all-carbon molecular switch based on a nanotube-fullerene-nanotube hybrid system [18]. They predicted that a large variation of the conductance over three orders of magnitude can be achieved by either changing the orientation of the fullerene molecule or rotating the nanotube.

[a] e-mail: tsli@mail.ksu.edu.tw

Electronic transport through nanometer-sized structures is one of the recent fundamental issues in mesoscopic physics [19–23]. An important result is that for an one-dimensional conductor in the ballistic regime, the electrical conductance is quantized in multiples of the quantum $2e^2/h$ [19,20]. It has been speculated that similar behavior should exist for the thermal transport. Schwab and collaborators observed the quantum of the thermal conductance, $\kappa_o = \pi^2 k_B^2 T/3h$, in nanosized narrow wires [24]. Theoretical calculations show that a conducting single-walled CN has only two conducting channels, and predict that the electrical conductance will be $4e^2/h$ independent of radius and length [25,26]. The electronic transport in graphene nanoribbons exhibits many interesting phenomena such as zero-conductance Fano resonances [27], vacancy configuration dependent conduction [28], half-metallic transport [29], and valley filtering conduction [30]. In our previous work, the electronic properties of nanotube-ribbon hybrids made up of a single-walled carbon nanotube and a graphene nanoribbon are investigated by using the tight-binding method [31]. In this paper, the effects of an external electric field on such systems are explored. Furthermore, the electrical and thermal transport properties of nanotube-ribbon hybrids are studied within the ballistic regime. They can be calculated by using the Landauer-Buttiker formalism, which relates the conductance of a system to an independent electron scattering problem. The electron transport in nanotube-ribbon hybrids has not yet been considered according to our knowledge.

2 Theory

In this study, we consider a system with a nanotube lying above a graphene nanoribbon with width N_w. Two configurations: (I) a $(m, 0)$ zigzag nanotube and an armchair ribbon, and (II) an (m, m) armchair nanotube and a zigzag ribbon are explored. There are $4m + 2N_w$ carbon atoms in the primitive unit cell. Schematic plot of a nanotube-ribbon hybrid system made up of a $(24, 0)$ zigzag nanotube and a $N_w = 90$ armchair nanoribbon is depicted in Figure 1. The location of the nanotube is specified by x_{loc}, the ribbon dimer line or the zigzag line that is directly underneath the nanotube axis. The nanotube and the ribbon are regarded as different subsystems. Details of the model formulations are given in our previous work [32], in which the electronic properties of nanotube-ribbon hybrids at zero field are studied. In the presence of a transverse electric field, the onsite energy of the ith carbon atom in such hybrids will be perturbed by the amount $\delta E = -eFy_i$, where y_i is the coordinate of the ith carbon atom along the field direction. After solving for the state energy $E(F)$, one may proceed to calculate the transport properties.

We consider a nanotube-ribbon hybrid suspended between two reservoirs (macroscopic leads) (Fig. 2). The left and right reservoirs are assumed to have the chemical potentials and the temperatures of $(\mu + eV,\ T)$ and $(\mu,\ T + \Delta T)$, respectively. Making use of the Landauer-Buttiker formula, the net electric and thermal currents in

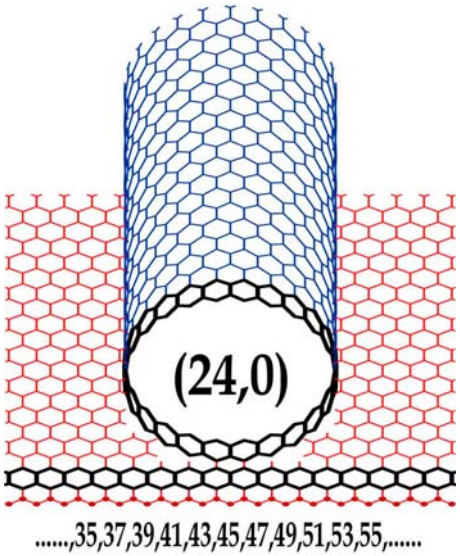

Fig. 1. (Color online) Schematic plot of a nanotube-ribbon hybrid made up of a $(24, 0)$ carbon nanotube and a $N_w = 90$ armchair graphene nanoribbon, $x_{loc} = 45$. The primitive unit cell is shown as heavy lines.

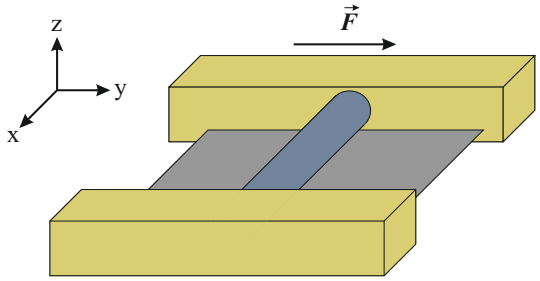

Fig. 2. (Colore online) Diagram of a nanotube-ribbon hybrid suspended between two leads. The electric field is along the y-axis.

the ballistic regime are respectively given by

$$I(F) = eT_o \int_{k>0} \frac{dk}{2\pi}\frac{1}{\hbar}\left|\frac{\partial E}{\partial k}\right|\left[f^o\left(\frac{E-\mu-eV}{T}\right) - f^o\left(\frac{E-\mu}{T+\Delta T}\right)\right] \quad (1)$$

and

$$U(F) = T_o \int_{k>0} \frac{dk}{2\pi}\frac{1}{\hbar}\left|\frac{\partial E}{\partial k}\right|(E-\mu)\left[f^o\left(\frac{E-\mu-eV}{T}\right) - f^o\left(\frac{E-\mu}{T+\Delta T}\right)\right], \quad (2)$$

where $(1/\hbar)\ |\ \partial E/\partial k\ |$ is the longitudinal velocity, T_o is the transmission probability for electrons in the reservoirs to enter the nanotube-ribbon hybrid with the above velocity and is just equal to 1 for an adiabatic contact. f^o is the Fermi-Dirac distribution function. Within the linear-response approximation ($\Delta T \to 0$ and $V \to 0$), I is reduced to $\mathcal{L}_0 V - (\mathcal{L}_1 \Delta T/T)$ and U becomes

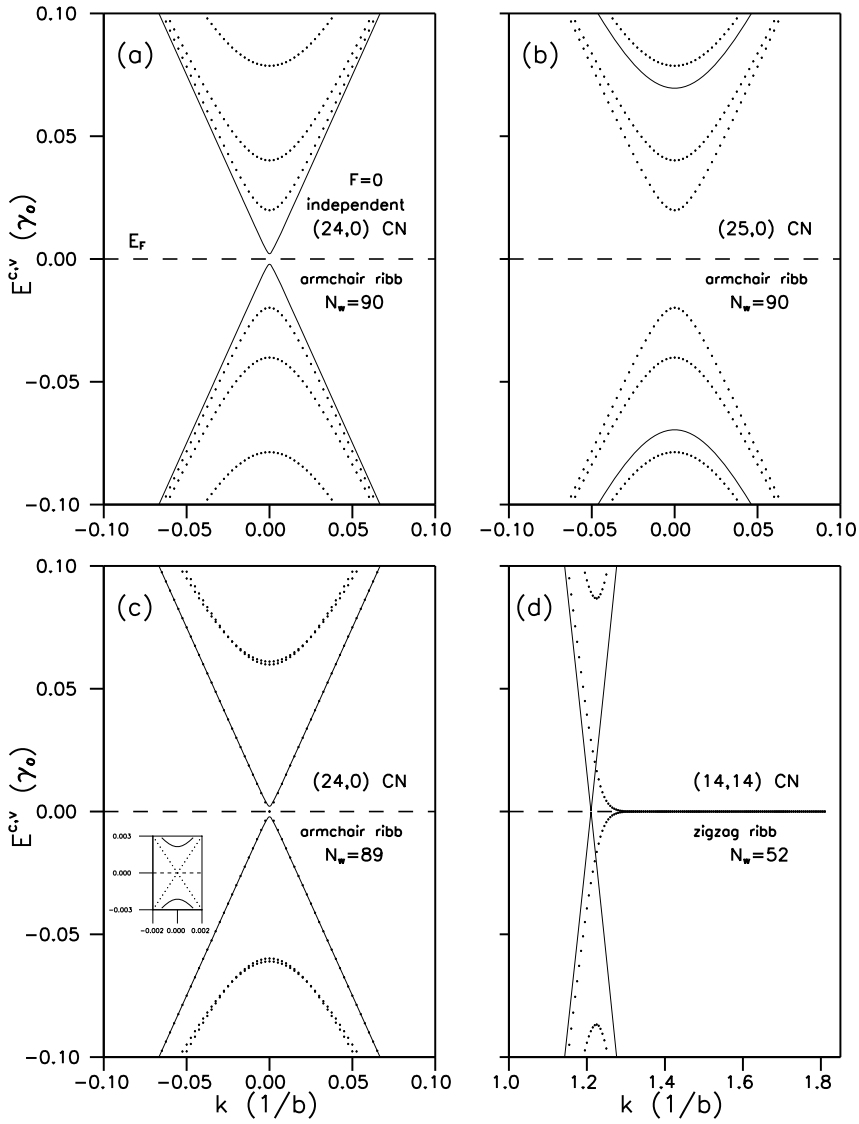

Fig. 3. The low-energy subbands without nanotube-ribbon interactions (independent subsystems) for (a) $(24,0)$ CN and $N_w = 90$ armchair ribbon, (b) $(25,0)$ CN and $N_w = 90$ armchair ribbon, (c) $(24,0)$ CN and $N_w = 89$ armchair ribbon, and (d) $(14,14)$ CN and $N_w = 52$ zigzag ribbon. The subbands of CN are shown as solid lines, and those of ribbon are displayed as dots. $\gamma_0 = 2.66$ eV is the nearest-neighbor transfer integral.

$\mathcal{L}_1 V - (\mathcal{L}_2 \Delta T/T)$. The electrical conductance is defined as $G = I/V = \mathcal{L}_0$ at $\Delta T = 0$. The thermal conductance κ, is the net thermal current produced by a temperature gradient at $I = 0$, and is given by $(\mathcal{L}_2 - \mathcal{L}_1^2 \mathcal{L}_0^{-1})/T$. $\mathcal{L}_\beta(F)$ is defined as

$$\mathcal{L}_\beta(F) = \frac{e^{2-\beta} T_o}{h} \int_{k>0} dk \left| \frac{\partial E}{\partial k} \right| (E-\mu)^\beta \frac{-\partial f^o(E)}{\partial E}. \quad (3)$$

At low temperature, the main contributions to $\mathcal{L}_\beta$ ($\beta = 0, 1, 2$) come from electronic states very close to the chemical potential.

3 Results and discussion

Four nanotube-ribbon hybrids: (I) $(24,0)$ CN and $N_w = 90$ armchair ribbon, (II) $(25,0)$ CN and $N_w = 90$ armchair ribbon, (III) $(24,0)$ CN and $N_w = 89$ armchair ribbon, and (IV) $(14,14)$ CN and $N_w = 52$ zigzag ribbon, are chosen to be part of a model study. The (24, 0), $(25,0)$, and $(14,14)$ CNs have roughly the same radii, although they belong to different categories of nanotubes. The $(24,0)$ CN is a narrow-gap semiconductor, whereas the $(25,0)$ CN is a moderate-gap semiconductor, and the $(14,14)$ CN is gapless. The $N_w = 90$ ($E_g > 0$), 89 ($E_g = 0$) armchair ribbons, and $N_w = 52$ ($E_g = 0$) zigzag ribbon have nearly the same width.

The bandstructures of nanotube-ribbon hybrids are briefly reviewed here. When nanotube and ribbon are decoupled (independent subsystems), the state energies are symmetric about the Fermi level $E_F = 0$ for all four hybrids (Fig. 3). In particular, there are partial flat bands at $E = 0$ with $\pi/3b < k \leq \pi/2b$ for hybrid (IV) (Fig. 3d).

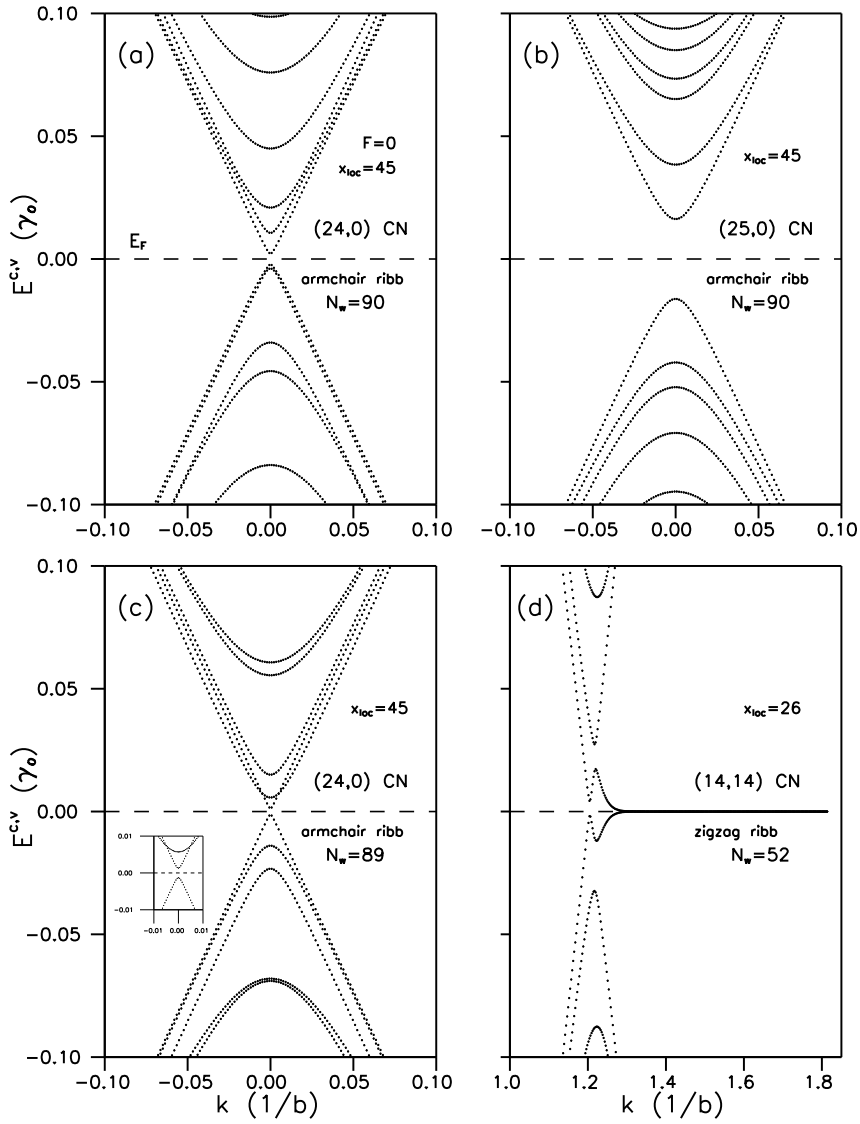

Fig. 4. The low-energy subbands with nanotube-ribbon interactions for (a) $(24,0)$ CN and $N_w = 90$ armchair ribbon (hydrid (I)), (b) $(25,0)$ CN and $N_w = 90$ armchair ribbon (hydrid (II)), (c) $(24,0)$ CN and $N_w = 89$ armchair ribbon (hydrid (III)), and (d) $(14,14)$ CN and $N_w = 52$ zigzag ribbon (hydrid (IV)).

These flat bands are contributed by the zigzag ribbon. At $k = \pi/2b$, the wavefunctions associated with the flat bands at $E = 0$ are the edge states at which the electrons are localized purely at the zigzag edges. With the inclusion of coupling, the bandstructures of all four hybrids are considerably altered, such as the modification of the subband curvature, the creation of additional band-edge states, and the change of subband spacing or energy gap (Fig. 4). Furthermore, the coupling will destroy the rotational symmetry of the nanotube, leading to the destruction of the state degeneracy. Finally, the energy bands are no longer symmetric about E_F. For hybrid (I), the lowest subbands originating from the $(24,0)$ CN are doubly degenerate. The second subbands are contributed by the ribbon (Fig. 3a). The nanotube-ribbon coupling lifts the double degeneray, reduces the energy gap, and changes the subband curvature or the k dependence of the state energy (Fig. 4a). For hybrid (II), the first and second subbands near E_F all belong to the $N_w = 90$ armchair ribbon, since $(25,0)$ CN is a moderate-gap semiconductor and its subbands are away from E_F (Fig. 3b). Nevertheless, the nanotube-ribbon hoppings will modify the lowest subbands considerably and reduce the energy gap (Fig. 4b). For hybrid (III), the linear subbands intersecting at E_F are contributed by the $N_w = 89$ armchair ribbon, and the second subbands (parabolic) originate from the $(24,0)$ CN (Fig. 3c). After turning on the nanotube-ribbon interactions, the subbands are strongly mixed, and linear subbands change into parabolic ones (Fig. 4c). For hybrid (IV), the linear subbands intersecting at E_F are contributed by the $(14,14)$ CN (Fig. 3d). They alter into parabolic bands with the influence of nanotube-ribbon coupling, and new band-edge

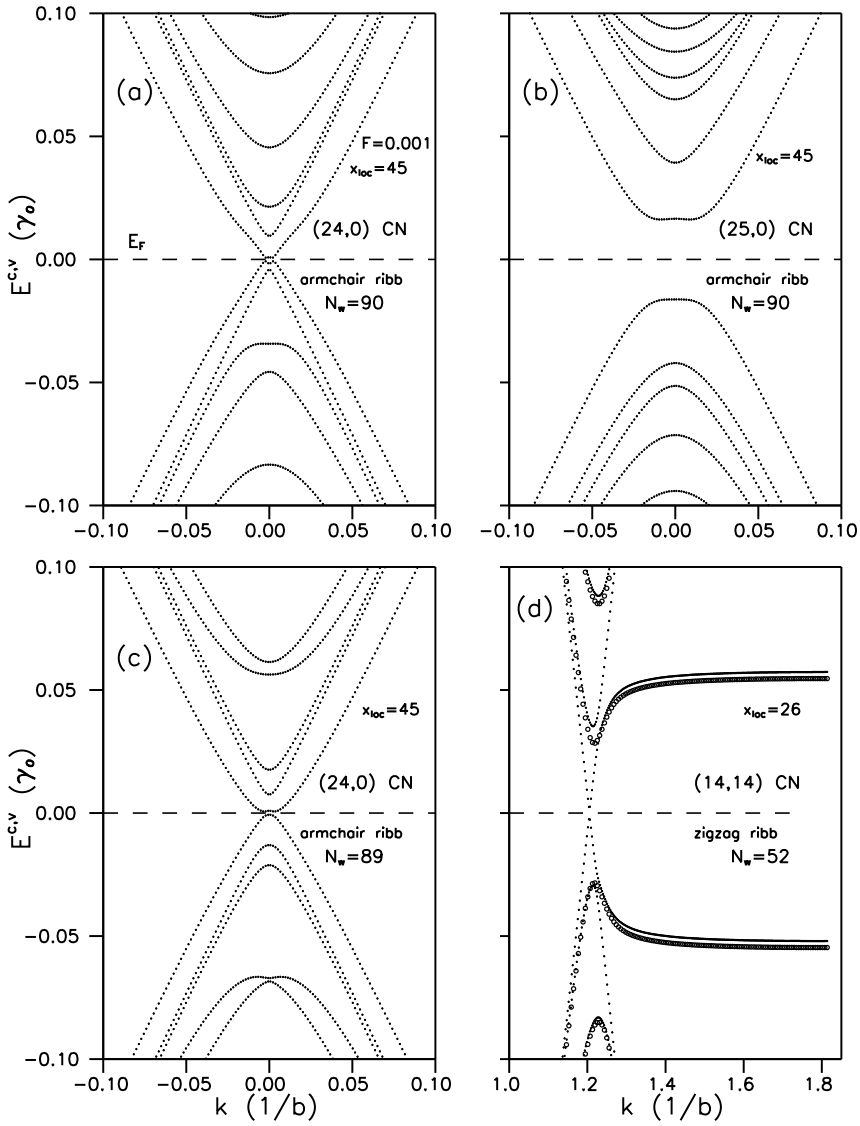

Fig. 5. The low-energy subbands of (a) $(24, 0)$ CN and $N_w = 90$ armchair ribbon (hydrid (I)), (b) $(25, 0)$ CN and $N_w = 90$ armchair ribbon (hydrid (II)), (c) $(24, 0)$ CN and $N_w = 89$ armchair ribbon (hydrid (III)), and (d) $(14, 14)$ CN and $N_w = 52$ zigzag ribbon (hydrid (IV)) at an external electric field. In (d), the low-energy subbands of $N_w = 52$ zigzag graphene nanoribbon are shown as circles.

states are created (Fig. 4d). The partial flat bands originating from the zigzag ribbon are almost unaffected by the nanotube-ribbon interactions, indicating that there is very weak or even no band hydridization between the ribbon and the nanotube in the flat bands. Finally, the energy gap stays at zero.

With the inclusion of a transverse electric field $F = 0.001\gamma_0/e$ Å, the subband curvatures and subband spacings are further altered. $\gamma_0 = 2.66$ eV is the nearest-neighbor transfer integral. New band-edge states are created (Fig. 5). The electric field opens a bandgap and lifts the partial flat bands degeneracy in hybrid (IV) (Fig. 5d). For comparison, we have also displayed the energy dispersons of the $N_w = 52$ zigzag graphene nanoribbon at the same F. For the zigzag graphene nanoribbon, the energy difference ΔE between the partial flat bands at $k = \pi/2b$ equals to $|eFw|$, where w is the width of the ribbon. In other words, ΔE is just the electrostatic energy difference between the electrons locating at the two zigzag edges. The partial flat bands characteristics of hybrid (IV) in an electric field closely resemble those of the $N_w = 52$ zigzag graphene nanoribbon. Our previous statement on the weak band hydridization between the ribbon and the nanotube in the flat bands can be extended to the case of nonzero electric field.

The energy gap of nanotube-ribbon hybrids varies sensitively with x_{loc} (Fig. 6a). When x_{loc} is not an integer, it signifies that the nanotube is locating somewhere between two adjacent ribbon dimer lines or zigzag lines . In general, the energy gap is oscillatory with x_{loc}. When the nanotube is lying at the middle of the ribbon, the geometry of the hybrid is left-right symmetrical. However, if the nanotube

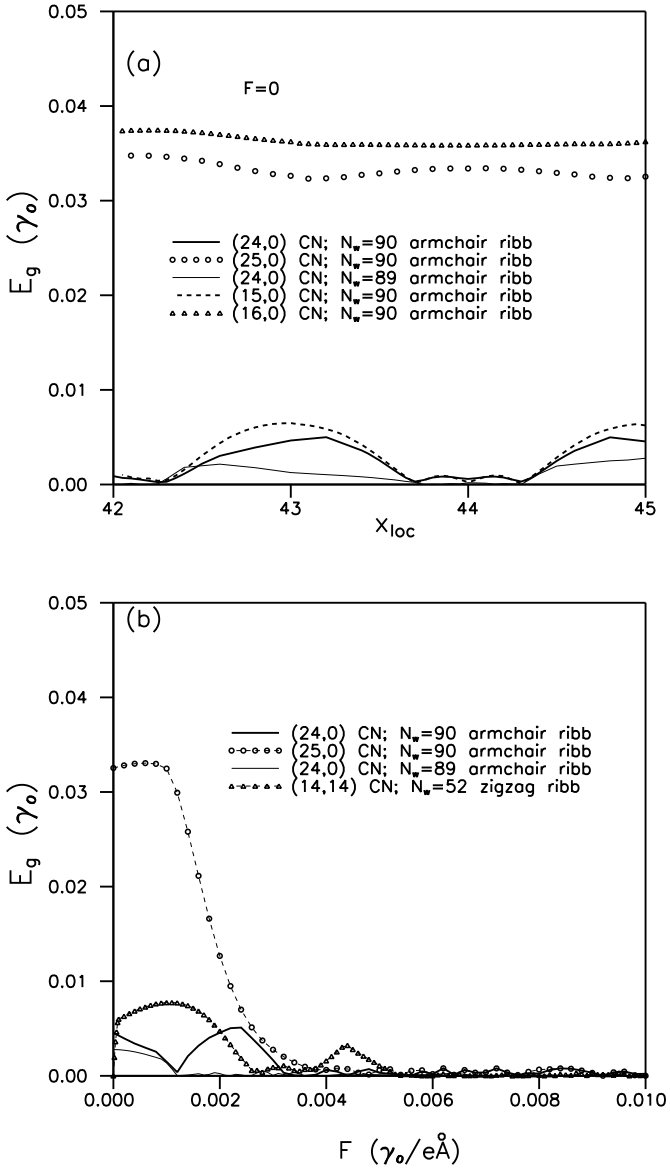

Fig. 6. (a) Energy gap dependence on x_{loc} for different nanotube-ribbon hybrids. When x_{loc} is not an integer, it signifies that the nanotube is locating somewhere between two adjacent ribbon dimer lines. (b) Energy gap dependence on F for different hybrids in which nanotubes are lying at the middle of the ribbons.

is displaced from the middle of the ribbon, such symmetry is lost. The variation of the bandgap with x_{loc} also signifies that the geometrical left-right symmetry could affect the electronic structures. For hybrids (I) and (III), the bandgaps touch the zero value at several x_{loc}'s and exhibit the semiconductor-metal transitions. The energy gap of hybrid (II) is also oscillating with varying x_{loc}, but there is no bandgap closing, for all x_{loc}'s. Finally, for hybrid (IV), the partial flat bands at E_F always exist, and the energy gap is always zero (not shown in (Fig. 6a) although the bandstructures have been noticeably modified by varying x_{loc}. It is of interest to investigate the effects of nanotube diameter on the energy gap. Both $(25, 0)$ and $(16, 0)$ CN's are moderate-gap semiconductors, and the diameter of the former is about one and a half times of the latter. Comparing their energy gap variation with x_{loc}, it is obvious that the bandgap of the $(25, 0)$ CN is usually smaller than that of the $(16, 0)$ CN at the same x_{loc}, and the amplitude of bandgap vibration of the former is larger that of the latter. We have also compared the bandgap of the narrow-gap $(24, 0)$ and $(15, 0)$ CN's. The bandgap of the former is generally smaller than that of the latter at the same x_{loc}. More importantly, bandgap closing occurs more frequently for the $(24, 0)$ CN. The explanation is as follows. For a larger nanotube, the atoms near the tube bottom are closer to the ribbon, leading to a stronger nanotube-ribbon coupling and the dependence on x_{loc}. The electronic structures of nanotube-ribbon hybrids vary sensitively with F, as is demonstrated by the F dependence of the bandgap (Fig. 6b). For hybrid (I), E_g first decreases to a very small value with increasing F, then rebounds, attains a peak value, and then shrinks to zero. For subsequent increases in F, E_g will oscillate with F. For hybrid (II), E_g increases slowly with F, reaches a maximum value, and then decreases rapidly. The bandgap of hybrid (III) is small and diminishes to zero as F rises, then fluctuates around zero with a small amplitude. Finally, even a very small F will open an energy gap in hybrid (IV), and this field-induced bandgap varies sensitively with F.

At very low temperature, the electrical conductance is proportional to the number of subbands intersecting with the chemical potential. The chemical-potential-dependent conductance therefore shows a step behaviour (Fig. 7a). Such steps appear whenever μ cross a subband. The stepwise increases with incrementing μ are due to the growing number of conducting subbands. Hydrids (I), (II) and (III) have about 276 subbands, while hydrid (IV) has only 160 subbands. Therefore, hydrid (IV) has less conductance steps than the others. The thermal conductance also displays a stepwise increase behavior (Fig. 7b) similar to that of the electrical conductance.

It is of interest to explore the influence of nanotube location (x_{loc}) on the conductance. For hybrid (I), the electrical conductance displays sharp peak structure at $x_{loc} =$ 42.3, 43.7 and 44.3. Explanations for this spiking behavior are as follows. The $\partial f^o(E)/\partial E$ function is a prominent Lorentzian function at the Fermi energy. Additionally, the electron state energies are very sensitive to x_{loc}. Therefore, whether the state closest to the Fermi level may contact E_F and thus contribute to the electrical conductance, or may not contact E_F and thus not contribute, depends very strongly on x_{loc}. The positions of the peak correspond to the x_{loc} values that lead to semiconductor-metal transitions, and their heights are related to the number of subbands at the Fermi level. The variation of the conductance with x_{loc} also signifies that the conductance relies on the geometrical left-right symmetry. For hybrid (II), there is no subband that crosses E_F for any values of x_{loc} resulting in zero conductance (not shown in (Fig. 8a). The thermal conductance behaves similarly to the electrical one (Fig. 8b).

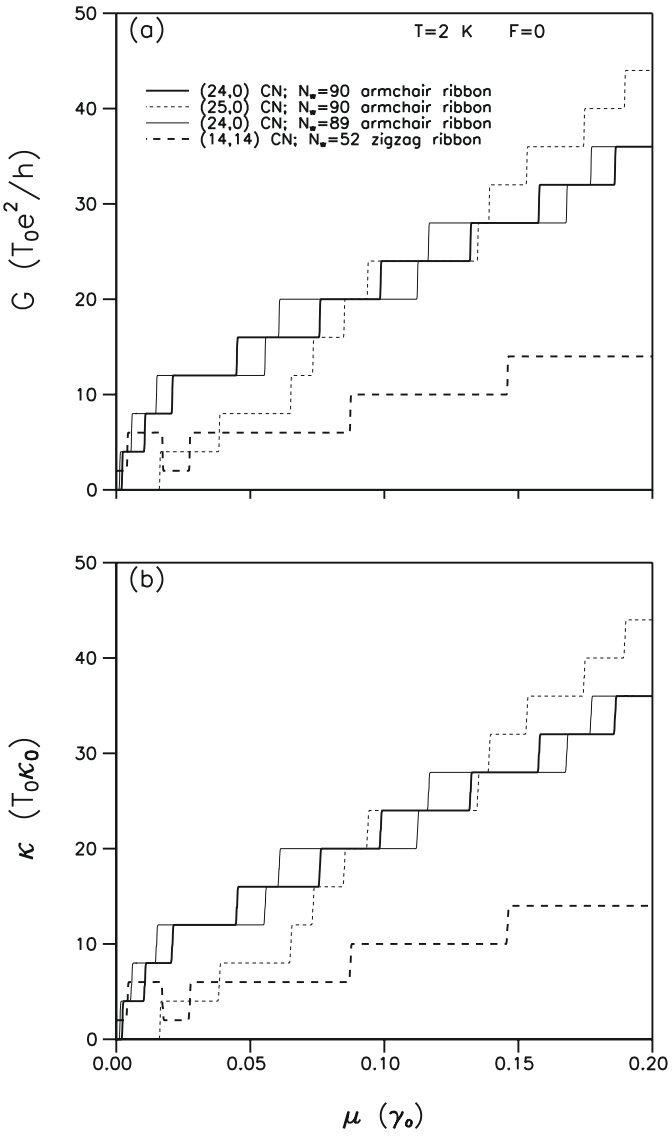

Fig. 7. Dependence of (a) the electrical conductance, and (b) the thermal conductance on the chemical potential μ for different nanotube-ribbon hybrids at $T = 2$ K and $F = 0$.

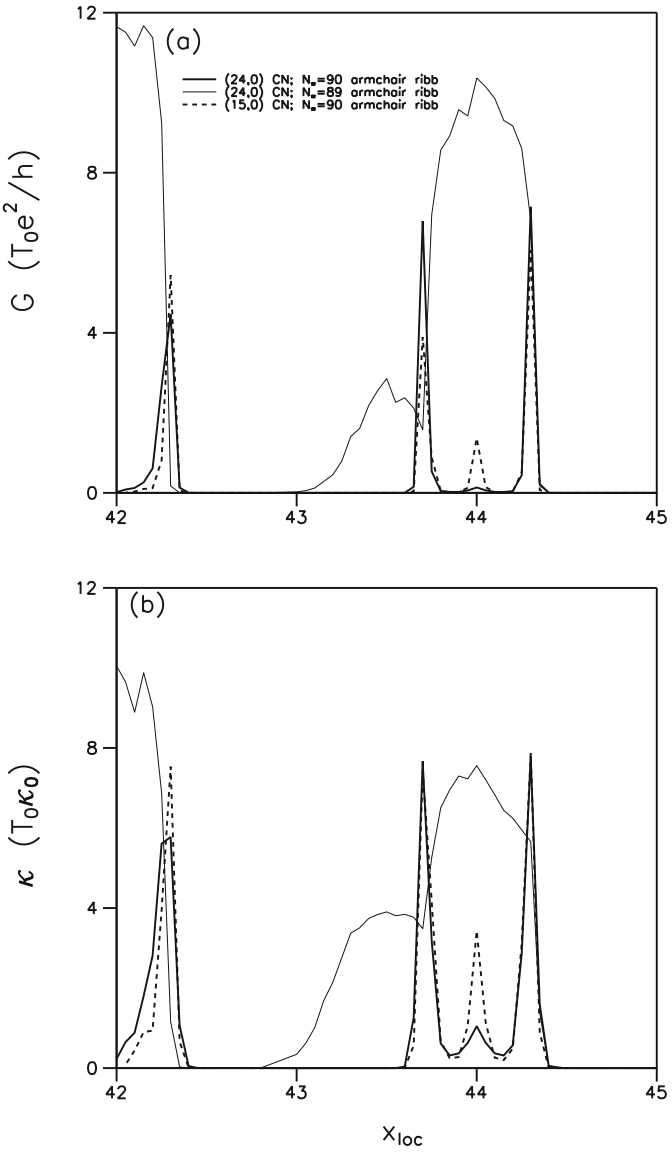

Fig. 8. Dependence of (a) the electrical conductance, and (b) the thermal conductance on x_{loc} for different nanotube-ribbon hybrids at $T = 2$ K and $F = 0$.

Field-induced conductance change is one of the most important issues in nanoelectronics [32,33]. For all four nanotube-ribbon hybrids, G is large at large F indicating that there are many subbands at E_F. Sharp peaks, as well as single-shoulder and multi-shoulder structures in the electrical conductance are demonstrated when varying F (Fig. 9a). The electrical conductance of hybrid (I) exhibits a small peak structure at $F = 0.0014\gamma_0/e$ Å, a boardened peak structure around $F = 0.0035\gamma_0/e$ Å and a combination of single-shoulder and peak structure at large F. The electrical conductance of hybrid (III) display a multi-shoulder structure. Its value plateaus at $12\ T_0e^2/h$ over the region ($0.0013\gamma_0/e$ Å $\leq F \leq 0.0035\gamma_0/e$ Å). There are always six subbands at the Fermi energy in that plateau region. Although varying F will modify the energy dispersion relationships accordingly, it does not change the number of bands at the Fermi energy, which is the only factor that determines the conductance. The thermal conductance curves closely resemble the electrical ones (Fig. 7b), and the slight difference between them originates from the different integrands in equation (3).

The thermal broadening effects on the conductance are shown in Figure 10. The $\partial f^o(E)/\partial E$ prominent Lorentzian function is widened due to the finite temperature resulting in a width k_BT, and consequently the number of conducting subbands is also changed. The shoulder structures of the electrical conductance and thermal conductance are gradually stretched by the increasing temperature. At the same temperature, the integrand of $\mathcal{L}_2$ (Eq. (3)), which is quadratic in $E - \mu$, is more extended in the energy domain than that of $\mathcal{L}_0$. Therefore, κ is more susceptible to the thermal broadening effects than G. We anticipate that quantum conductance

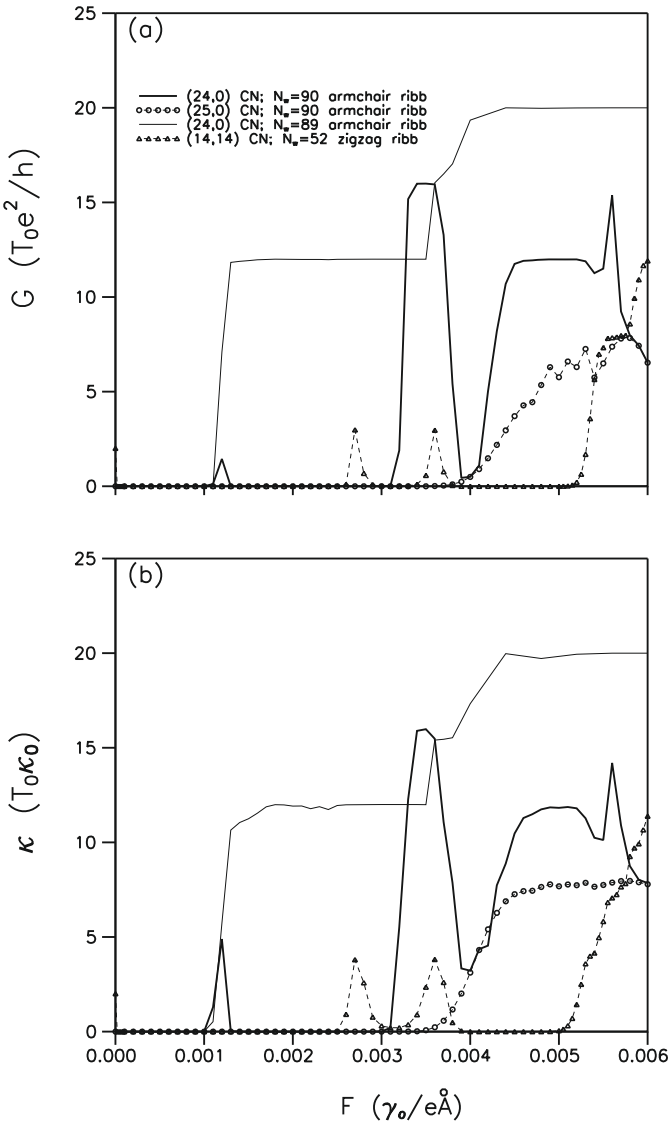

Fig. 9. Dependence of (a) the electrical conductance, and (b) the thermal conductance on F for different nanotube-ribbon hybrids at $T = 2$ K. The nanotubes are lying at the middle of the ribbon.

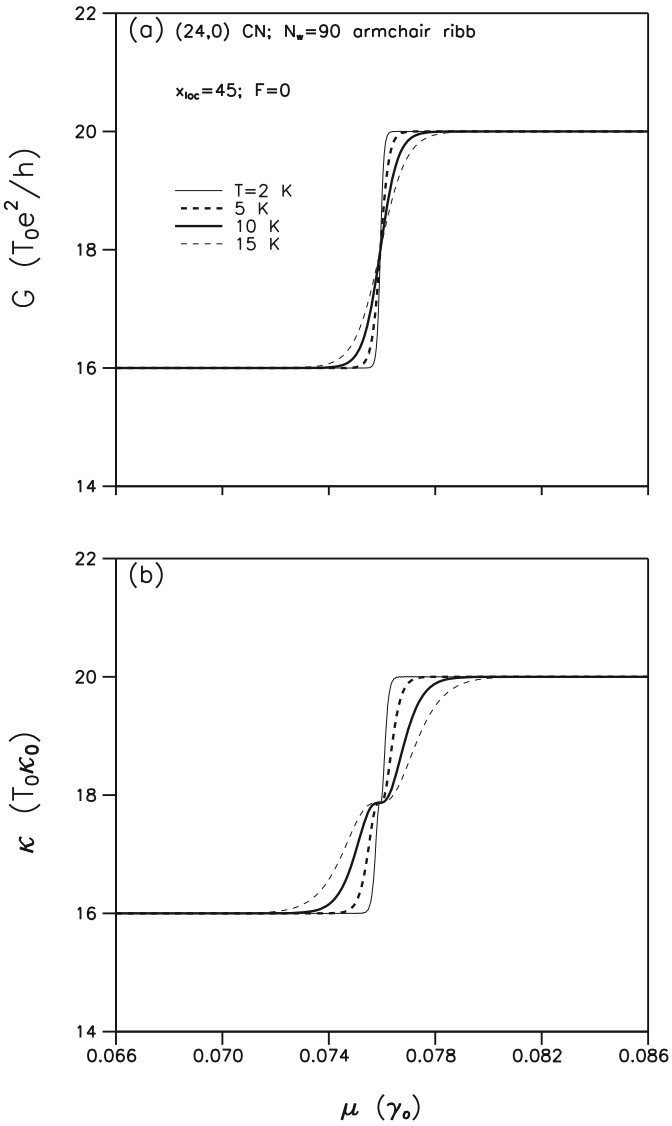

Fig. 10. Dependence of (a) the electrical conductance, and (b) the thermal conductance, on the chemical potential μ for hybrid (I) at various temperatures.

behavior in nanotube-ribbon hybrids can be observed experimentally at temperature around 10 K. Depolarization or screening effects, which arise from redistribution of carriers induced by the external electric field, have not been taken in account. A thorough investigation of the effective electric field would require the self-consistent field approach [34,35]. In this study, F is the effective electric field strength, and the external (or applied) electric field strength is roughly determined to be five times of F in a carbon nanotube, according to calculations given in literatures [36–38].

4 Concluding remarks

In conclusion, the tight-binding model has been employed to study the electronic and transport properties of nanotube-ribbon hybrids. The energy dispersion relations are found to exhibit rich dependence on the nanotube-ribbon interactions, the field strength, and the geometry of the hybrids. The nanotube-ribbon coupling will modify the subband curvature, create additional band-edge states, and change the subband spacing or energy gap. The bandstructures are asymmetric and symmetric about the Fermi energy when the interactions are turned on and off, respectively. The inclusion of a transverse electric field will further alter the bandstructures and lift the degeneracy of the partial flat bands in hybrid (IV). The chemical-potential-dependent electrical and thermal conductance exhibit a stepwise increase behavior. Variations in the electronic structures with field strength will be reflected in the electrical and thermal conductance. Prominent peaks, as well as single-shoulder and multi-shoulder

structures in the electrical and thermal conductance are predicted when varying the electric field strength and the nanotube location. The features of the conductance are found to be strongly dependent on the field strength, the geometry and the temperature. These theoretical predictions can be verified by conductance measurements.

This work was supported in part by the National Science Council of Taiwan, the Republic of China under Grant No. NSC 97-2112-M-168-002.

References

1. S. Iijima, Nature **354**, 56 (1991)
2. R. Saito, M. Fujita, G. Dresselhaus, M.S. Dresselhaus, Appl. Phys. Lett. **60**, 2204 (1992)
3. J.W.G. Wildoer, L.C. Venema, A.G. Rinzler, R.E. Smalley, C. Dekker, Nature **391**, 59 (1998)
4. T.W. Odom, J.L. Huang, P. Kim, C.M. Lieber, Nature **391**, 62 (1998)
5. H.W. Kroto, J.R. Heath, S.C. O'Brien, R.F. Curl, R.E. Smalley, Nature **318**, 162 (1985)
6. K.S. Novoselov, A.K. Geim, S.V. Morozov, D. Jiang, Y. Zhang, S.V. Dubonos, I.V. Grigorieva, A.A. Firsov, Science **306**, 666 (2004)
7. C. Berger, Z.M. Song, T.B. Li, X.B. Li, A.Y. Ogbazghi, R. Feng, Z.T. Dai, A.N. Marchenkov, E.H. Conrad, P.N. First, W.A. de Heer, J. Phys. Chem. B **108**, 19912 (2004)
8. K.S. Novoselov, A.K. Geim, S.V. Morozov, D. Jiang, M.I. Katsnelson, I.V. Grigorieva, S.V. Dubonos, A.A. Firsov, Nature **438**, 197 (2005)
9. Y. Zhang, J.P. Small, M.E.S. Amori, P. Kim, Phys. Rev. Lett. **94**, 176803 (2005)
10. J.S. Bunch, Y. Yaish, M. Brink, K. Bolotin, P.L. McEuen, Nano. Lett. **5**, 2887 (2005)
11. Y. Zhang, J.P. Small, W.V. Pontius, P. Kim, Appl. Phys. Lett. **86**, 073104 (2005)
12. Y. Zhang, Y.W. Tan, H.L. Stormer, P. Kim, Nature **438**, 201 (2005)
13. K.S. Novoselov, E. McCann, S.V. Morozov, V.I. Falko, M.I. Katsnelson, U. Zeitler, D. Jiang, F. Schedin, A.K. Geim, Nat. Phys. **2**, 177 (2006)
14. C. Berger, Z. Song, X. Li, X. Wu, N. Brown, C. Naud, D. Mayou, T. Li, J. Hass, A.N. Marchenkov, E.H. Conrad, P.N. First, W.A. de Heer, Science **312**, 1191 (2006)
15. B.W. Smith, M. Monthioux, D.E. Luzzi, Nature **396**, 323 (1998)
16. A.G. Nasibulin, P.V. Pikhitsa, H. Jiang, D.P. Brown, A.V. Krasheninnikov, A.S. Anisimov, P. Queipo, A. Moisala, D. Gonzalez, G. Lientschnig, A. Hassanien, S.D. Shandakov, G. Lolli, D.E. Resasco, M. Choi, D. Tomanek, E.I. Kauppinen, Nat. Nano. **2**, 156 (2007)
17. X. Zhao, Y. Ando, Y. Liu, M. Jinno, T. Suzuki, Phys. Rev. Lett. **90**, 187401 (2003)
18. R. Gutierrez, G. Fagas, G. Cuniberti, F. Grossmann, R. Schmidt, K. Richter, Phys. Rev. B **65**, 113410 (2002)
19. R. Landauer, IBM J. Res. Dev. **1**, 223 (1957)
20. R. Landauer, Philos. Mag. **21**, 863 (1970)
21. B.J. van Wees, H. van Houten, C.W.J. Beenakker, J.G. Williamson, L.P. Kouwenhoven, D. van der Marel, C.T. Foxon, Phys. Rev. Lett. **60**, 848 (1988)
22. W.J. Skocpol, P.M. Mankiewwich, R.E. Howard, L.D. Jackel, D.M. Tennant, A.D. Stone, Phys. Rev. Lett. **56**, 2865 (1986)
23. Datta, *Electronic Transport in Mesoscopic Systems* (Cambridge University Press, Cambridge, England, 1995)
24. K. Schwab, E.A. Henriksen, J.M. Worlock, M.L. Roukes, Nature **404**, 974 (2000)
25. M.F. Lin, K.W.K. Shung, Phys. Rev. B **51**, 7592 (1995)
26. L. Chico, L.X. Benedict, S.G. Louie, M.L. Cohen, Phys. Rev. B **54**, 2600 (1996)
27. K. Wakabayashi, M. Sigrist, Phys. Rev. Lett. **84**, 3390 (2000)
28. K. Wakabayashi, J. Phys. Soc. Jpn **71**, 2500 (2002)
29. Y.W. Son, M.L. Cohen, S.G. Louie, Nature **444**, 347 (2006)
30. A. Rycerz, J. Tworzydlo, C.W.J. Beenakker, Nat. Phys. **3**, 172 (2007)
31. T.S. Li, S.C. Chang, J.Y. Lien, M.F. Lin, Nanotechnology **19**, 105703 (2008)
32. P.W. Chiu, M. Kaempgen, S. Roth, Phys. Rev. Lett. **92**, 246802 (2004)
33. C.W.J. Beenakker, H. van Houten, Solid State Phys. **44**, 1 (1991)
34. H. Ehrenreich, M.H. Cohen, Phys. Rev. **115**, 786 (1959)
35. T.S. Li, M.F. Lin, J. Phys. Soc. Jpn **74**, 425 (2005)
36. Y. Li, V. Rotkin, U. Ravaioli, Nano. Lett. **3**, 183 (2003)
37. C. Chen, W.C. Hseih, M.F. Lin, Phys. Rev. B **72**, 193412 (2005)
38. L.X. Benedict, S.G. Louie, M.L. Cohen, Phys. Rev. B **52**, 8541 (1995)